



## Article

# Determination of Paleoenvironmental Changes by Using $\delta^{13}\text{C}$ , $^{14}\text{C}$ Dating and Rb/Sr Ratio in Critical Karst Area of Yunnan-Guizhou Plateau, Southwestern China

Howard Omar Beckford <sup>1</sup>, Cheng Chang <sup>1</sup> and Hongbing Ji <sup>1,2,\*</sup>

<sup>1</sup> School of Energy and Environmental Engineering, University of Science and Technology Beijing, Beijing 100083, China

<sup>2</sup> State Key Laboratory of Environmental Geochemistry, Institute of Geochemistry, Chinese Academy of Sciences, Guiyang 550002, China

\* Correspondence: ji.hongbing@hotmail.com; Tel./Fax: +86-10-6233-2750

**Abstract:** Paleosols preserve archives of vegetation history, environmental changes, and sedimentary systems. The changes in vegetation history and environmental conditions in karst areas of the Yunnan–Guizhou plateau of southwestern China since the late Pleistocene were analyzed using  $\delta^{13}\text{C}$ ,  $^{14}\text{C}$  and the Rb/Sr ratio. Our  $\delta^{13}\text{C}$  results reveal the coexistence of C3 and C4 plants (−10.91 to −30.45‰) in soil organic matter, something that is consistent with the present field vegetation assessment. The large vertical difference in the  $\delta^{13}\text{C}$  value (>4‰) is related to the cultivation of agricultural crops and to changes in environmental conditions. Furthermore, the variation in  $\delta^{13}\text{C}$  values was influenced by the summer monsoon climate of the Indian Ocean and east Asia. We found that total organic carbon (TOC) concentration decreased exponentially with soil depth, indicating high carbon loss. In addition,  $^{14}\text{C}$  apparent age of the soil profiles ranged from modern times to 20,605 ( $\pm 63$ ) years before the present (yrs. BP) and is positively correlated with soil depth. The combined results indicate that, since the late Pleistocene era, environmental conditions in the study area have changed intermittently on a scale of millennia from hot-humid to cold-dry conditions. We speculate that there may have been extreme climate events in the study area 14,750 years BP, which are marked by a drastic change in  $\delta^{13}\text{C}$  and in the Rb/Sr ratio.

**Keywords:** climate change; carbon isotope; trace elements; Yunnan-Guizhou plateau; southwestern China



**Citation:** Beckford, H.O.; Chang, C.; Ji, H. Determination of Paleoenvironmental Changes by Using  $\delta^{13}\text{C}$ ,  $^{14}\text{C}$  Dating and Rb/Sr Ratio in Critical Karst Area of Yunnan-Guizhou Plateau, Southwestern China. *Sustainability* **2023**, *15*, 6480. <https://doi.org/10.3390/su15086480>

Academic Editor: Vinicio Manzi

Received: 22 February 2023

Revised: 27 March 2023

Accepted: 31 March 2023

Published: 11 April 2023



**Copyright:** © 2023 by the authors. Licensee MDPI, Basel, Switzerland. This article is an open access article distributed under the terms and conditions of the Creative Commons Attribution (CC BY) license (<https://creativecommons.org/licenses/by/4.0/>).

## 1. Introduction

Paleosols are important paleo-ecological archives as they preserve records of earth's past critical zones and the in situ substrate of ancient landscapes [1–5]. Many researchers over the years have used isotopes and geochemical methods in paleopedology and paleoenvironmental reconstruction to understand the environment [6–14]. Presently, with the rapidly increasing demand of resources it is imperative to understand the earth's past and present environments and processes, especially in ecologically fragile karst environments. The Yunnan–Guizhou plateau, of southwestern China, forms one of the largest continuously developed ancient weathering crusts on the earth's surface [15,16] and little paleoecology information is currently available. Therefore, our approach is to examine changes in several soil profiles over carbonate weathering crust by using  $\delta^{13}\text{C}$  and  $^{14}\text{C}$  dating and Rb/Sr ratios. Stable carbon composition ( $\delta^{13}\text{C}$ ) of soil organic matter (SOM) registers information regarding the occurrence of C3 and C4 plant species in plant communities. The  $\delta^{13}\text{C}$  values of SOM are inherited from present vegetation cover, with C3 and C4 plant  $\delta^{13}\text{C}$  values usually considered to range between −23‰ and −30‰ (avg. −27‰) and between −9‰ and −17‰ (avg. −13‰) respectively [17]. Therefore, C3 and C4 plants have distinct  $\delta^{13}\text{C}$  values which differ from each other by approximately 14‰ [17]. Radioisotope  $^{14}\text{C}$  has

been used by several researchers as a tracer tool for use in the study of carbon cycling in different ecosystems [18–24] and in paleoenvironmental studies [21–24]. Generally, researchers have used sensitive biomarkers as indices to reflect climate or environmental change [25,26]. However, other useful geochemical proxies, such as Rb/Sr ratios, can reflect rainfall variations and hence weathering intensities [27–29]. The alkali elements K and Rb are dominant in K-feldspars, in elite and in kaolinite mineral [30], and they have similar chemical characteristics that may function similarly in minerals [31]. The ionic potential of  $\text{Sr}^{2+}$  (1.8) is relatively similar to  $\text{Ca}^{2+}$  (2.0) [32] and so behaves chemically similar, as a result it readily substitutes for Ca in calcium carbonate [30]. However, different geochemical behaviors of the ratio of the element pair Rb and Sr in loess–paleosol can reflect weathering intensities and pedogenesis [33] as Rb tends to be immobile while Sr appears to be mobile during weathering and pedogenesis processes. High Rb/Sr can be interpreted to indicate hot–humid conditions that facilitate high weathering and leaching activities, while low Rb/Sr indicates cold–dry conditions and low leaching activities. This paper therefore used the combination of  $\delta^{13}\text{C}$ ,  $^{14}\text{C}$  dating and Rb/Sr ratio in carbonate weathering profiles to demonstrate paleoenvironmental changes in the Yunnan–Guizhou plateau of southwestern China.

## 2. Materials and Methods

### 2.1. Description of Study Area

The study area is the Yunnan–Guizhou plateau (YG) which is located in southwestern China (Figure 1). It covers approximately 500,000 km<sup>2</sup> and is one of the largest distributions of continuous karst in the world [34]. The terrain is composed of highlands to the east and low mountains to the west and encompasses Kunming and Guiyang City. The sample profiles are distributed along an altitudinal gradient ranging from 853 m to 1770 m. The Yunnan–Guizhou plateau experienced a typical subtropical monsoon climate with warm–humid conditions from May to October and cold–dry conditions from November to April. The average annual temperature and rainfall are 16.3 °C and 850–1600 mm, respectively, with relatively large temperature differences between day and night [34].

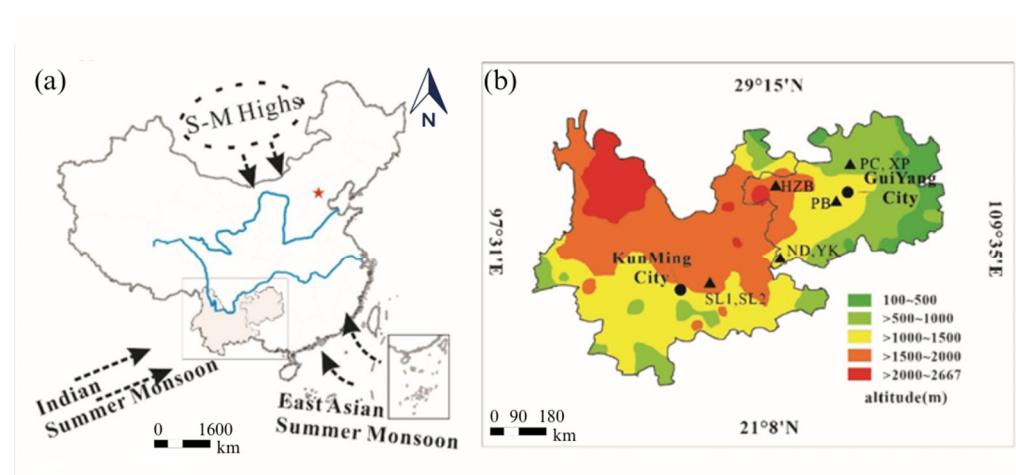


**Figure 1.** Map of China showing (a) the location of study area and (b) the location and position of sample profiles across elevation gradients at the Yunnan–Guizhou plateau of southwestern China.

The Yunnan–Guizhou plateau mainly consists of Proterozoic clastic sedimentary rocks and Paleozoic to upper-middle Triassic marine carbonate rocks, with post Triassic rocks and fluvial deposits [35]. The period was dominated by Equatorial and east Asian summer monsoons and a Siberia–Mongolia winter monsoon [35]. These monsoonal climates strongly influenced soil distribution, with red soil dominant in the western region while yellow soil occurred in the eastern region. The predominant soil types from the region are characterized

as red soil and limestone soil [36–38]. Based on the United States Department of Agriculture (USDA) soil taxonomy classification system, soils developed from limestone are classified as Mollic Inceptisols [39].

## 2.2. Soil Profile and Sample Collection

The study sites were identified through remote sensing research and field investigation according to soil type and geological distribution map. There are a total of eight (8) soil profiles across a wide elevation range that represents high mountains in the east to low mountains in the west of the Yunnan-Guizhou plateau. Limestone and dolomite bedrocks were selected and measured (Figure 1).

The locations of the soil profiles, elevation, thickness, parent material and visible characteristics are presented in Table 1. The studied profiles vary in depth from 50–220 cm with usually three distinct soil layers. According to the characteristics of the studied profiles, the section is divided into three layers: layer A (topsoil layer); layer B (weathering layer or regolith); and layer C, which is subdivided into C1 (rock powder layer), C2 (weathered rock layer) and C3 (bedrock). However, not all of the soil profiles have all of the layers, for example, the rock powder layer is only found in the dolomite weathering profile. Photograph and diagrammatic representation of each profile is illustrated in Figures 2 and 3, respectively. Mineral compositions of the sample profiles are reported in the studies by Ji et al., 2020 [40] and Chang et al., 2022 [41], the XRD results of which indicate that the main mineral component of the profiles are quartz and clay minerals such as illite, montmorillonite, and kaolinite. However, iron-bearing minerals, such as magnetite and hematite, are also present. Gibbsite was also found in all profiles, indicating that the profiles have experienced strong weathering.

**Table 1.** Soil profile, location, elevation, thickness, parent material and visible characteristics for the studied profiles from karst areas in the Yunnan-Guizhou plateau of southwestern China.

Soil Profiles	Location	Elevation (m)	Thickness (cm)	Parent Material	Soil Texture	Visible Characteristics
SL1	24°48′ N; 103°18′ E	1770	50	Limestone	Silty clay loam	Dark brown
SL2	24°48′ N; 103°18′ E	1730	113	Limestone	Silty loam	Red
ND	24°49′ N; 104°51′ E	1279	190	Carbonate	Silty loam	Red
YK	24°49′ N; 104°51′ E	1116	100	Carbonate	Silty clay loam	Reddish brown
PC	27°51′ N; 107°02′ E	951	220	Limestone lower Triassic	Silty clay loam	Yellowish brown
XP	27°44′ N; 107°03′ E	853	150	Dolomite upper Cambrian	Clayey loam	Red brown
PB	26°25′ N; 106°21′ E	1256	200	Dolomite lower Triassic	Silty loam	Red
HZB	27°08′ N; 104°43′ E	1689	220	Limestone lower Permian	Silty clay loam	Yellowish brown

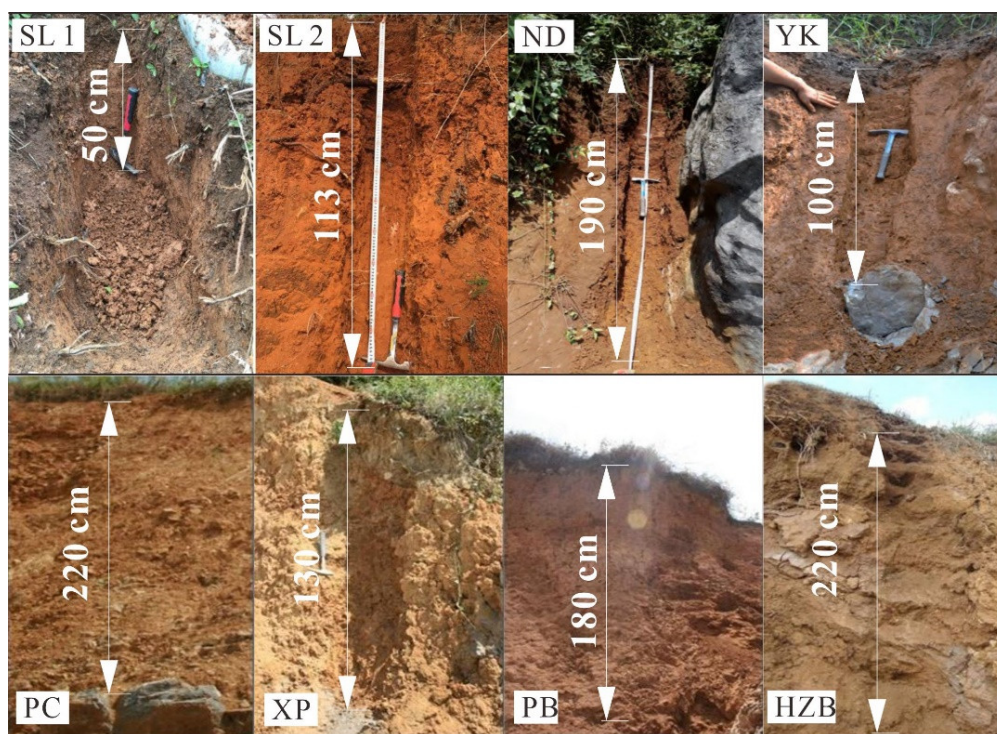


Figure 2. Photographs of the weathering profiles from Yunnan-Guizhou Plateau, Southwestern China.

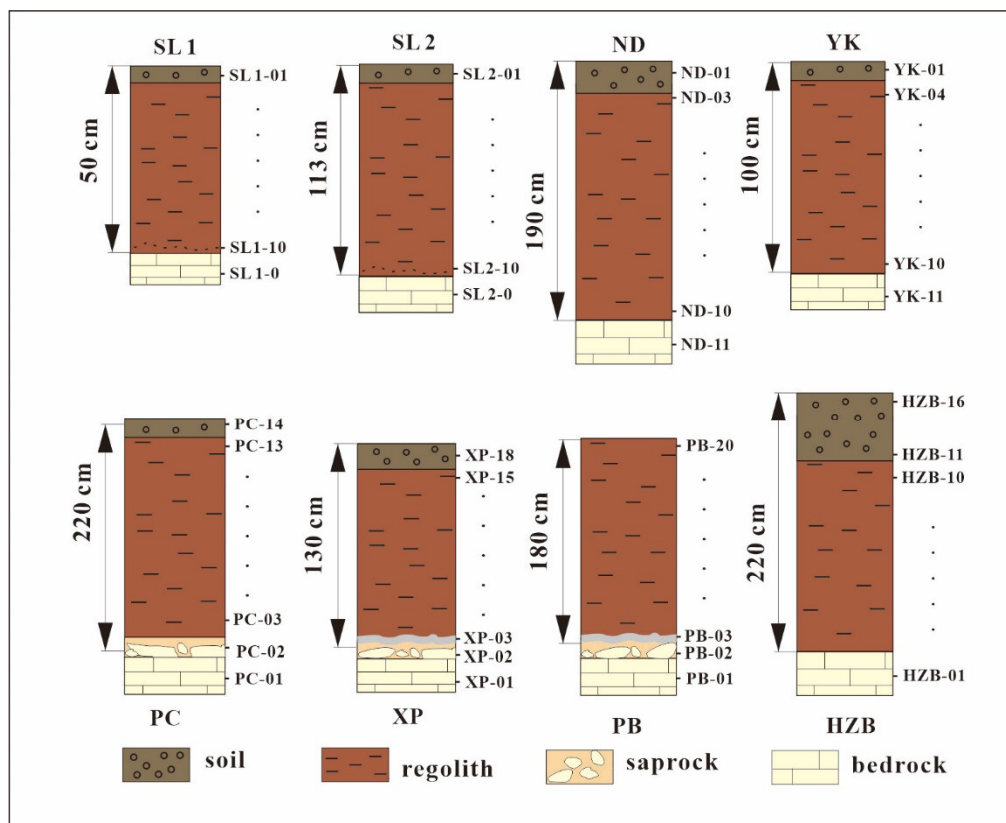


Figure 3. Diagrammatic representation of the sample profiles at the Yunnan-Guizhou plateau of southwestern China.

The surrounding upland vegetation mainly consists of terrestrial C3 and C4 plants which include native plants, shrubs, ferns and herbaceous plants. Some common plants species that dominated the SL1, SL2, ND and YK profiles were *Ligustrum lucidum*, *Pinus massoniana*, *Eucommia ulmoides*, *Pinus elliottii*, and *Artemisia annua*. Meanwhile the plant species that dominated the PC and XP profiles were mainly shrubs, cultivated corn, *Artemisia scoparia* and *Ligustrum lucidum*. The plant species that dominated the PB and HZB profiles were mainly *Pinus massoniana*, *Eucommia ulmoides*, *Pteridium aquilinum*, *Miscanthus floridulus* and *Imperata cylindrica*. A channeling sampling method was employed to collect samples from the bottom to the top of the profile. Fresh soil samples were collected at intervals ranging between 0 and 20 cm according to the genetic horizons of each profile. Each soil sample was carefully numbered and labeled based on sample location and position e.g., SL1-1 to SL1-10. Additionally, respective bedrock from each profile were also collected, numbered and labeled accordingly (Table 2).

**Table 2.** Soil depth distribution with pH, TOC,  $\delta^{13}\text{C}$ ,  $^{14}\text{C}$ , Rb/Sr concentration and ratios for studied soil profiles from karst areas in the Yunnan-Guizhou plateau of southwestern China.

Sample Profiles	Soil Depth (cm)	pH	TOC (%)	$\delta^{13}\text{C}$ (‰)	pMC (%)	Error (1 $\sigma$ )	$^{14}\text{C}$ Age (yrs BP)	Error (1 $\sigma$ )	Rb ( $\mu\text{g/g}$ )	Sr ( $\mu\text{g/g}$ )	Rb/Sr
SL1-1	5	5.99	0.286	−16.831	94	0.23	500	20	93.7	24	3.90
SL1-2	10	6.025	2.255	−16.517					91.8	22.8	4.02
SL1-3	15	6.09	2.051	−16.008	92.59	0.24	620	20	97.8	24.1	4.05
SL1-4	20	6.075	1.676	−15.984					94.7	24	3.94
SL1-5	25	6.015	1.764	−16.204	91.45	0.24	720	20	94.9	23.9	3.97
SL1-6	30	6.02	1.56	−16.367					99.2	24.9	3.98
SL1-7	35	6.055	1.372	−16.219	89.5	0.24	890	20	99.2	25.5	3.89
SL1-8	40	6.04	1.41	−16.345					95.9	24.8	3.86
SL1-9	45	5.995	1.157	−16.683	91.21	0.25	740	20	97.8	26.6	3.67
SL1-10	50	5.945	0.953	−16.874					91	24.6	3.69
SL1-0	100	nd	nd	nd					1.15	47.2	0.02
SL2-1	5	5.02	2.118	−20.698	98.92	0.26	90	20	78.5	19.7	3.98
SL2-2	17	5.065	0.729	−18.345	90.62	0.24	790	20	85.7	20.8	4.12
SL2-3	29	5.11	0.413	−18.103	81.71	0.26	1620	25	91.7	20.1	4.56
SL2-4	41	5.22	0.351	−18.34	82.77	0.26	1520	25	82.5	18.6	4.43
SL2-5	53	5.05	0.24	−19.307	68.47	0.2	3040	25	75.3	18.5	4.07
SL2-6	65	5.085	0.153	−20.001					70.7	18.7	3.78
SL2-7	77	5.445	0.154	−20.314					69.1	19.1	3.61
SL2-8	89	5.575	0.158	−21.001					71	19.6	3.62
SL2-9	101	5.255	0.16	−20.83					76	22.8	3.33
SL2-10	113	5.17	0.145	−21.696					81.1	21.8	3.72
SL2-0	163	nd	nd	nd					0.601	69.9	0.008
ND-1	0	6.79	2.835	−15.8	85.08	0.23	1300	20	116	84.4	1.37
ND-2	20	6.79	0.895	−16.1	47.68	0.23	5950	40	79.1	78.4	1.008
ND-3	40	6.71	0.669	−16.5	48.01	0.17	5895	30	89.3	83.2	1.073
ND-4	60	6.53	0.584	−16.6	39.84	0.16	7390	30	91.5	83.8	1.091
ND-5	80	6.46	0.583	−16.6	37.54	0.17	7870	35	115	82.2	1.39
ND-6	100	6.83	0.509	−16.8					108	74.8	1.44
ND-7	120	6.7	0.591	−17					108	73.8	1.46
ND-8	140	6.67	0.565	−17					114	78.1	1.45
ND-9	160	6.92	0.576	−17.1					109	82.4	1.32
ND-10	180	6.84	0.644	−17.3					102	80.1	1.27
ND-11	190	nd	nd	nd					6.43	200	0.03
YK-1	0	7.3	1.443	−14.8	71.99	0.21	2640	25	131	137	0.95
YK-2	10	7.12	0.612	−17.8					156	162	0.96
YK-3	20	6.9	0.521	−18	22.89	0.11	11845	40	143	162	0.88
YK-4	30	6.93	0.473	−18.3					145	157	0.92
YK-5	40	7.05	0.539	−18.5	19.76	0.11	13025	45	158	163	0.96
YK-6	50	7.09	0.542	−18.2					153	158	0.96
YK-7	60	7.05	0.433	−18.1	15.78	0.09	14835	45	152	172	0.88
YK-8	70	7.17	0.39	−18					166	155	1.07

Table 2. Cont.

Sample Profiles	Soil Depth (cm)	pH	TOC (%)	$\delta^{13}\text{C}$ (‰)	pMC (%)	Error (1 $\sigma$ )	$^{14}\text{C}$ Age (yrs BP)	Error (1 $\sigma$ )	Rb ( $\mu\text{g/g}$ )	Sr ( $\mu\text{g/g}$ )	Rb/Sr
YK-9	80	7.23	0.477	−17.8	23.46	0.12	11645	40	160	155	1.03
YK-10	90	7.47	0.511	−17.9					152	150	1.01
YK-11	100	nd	nd	nd					1.15	220	0.005
PC-14	0	6.8	2.33	−25.15	82.99	0.21	1498	20	88.3	64.4	1.37
PC-13	10	6.2	0.52	−18.29	45.09	0.15	6399	27	82.7	46.4	1.78
PC-12	30	6.1	0.35	−23.42					78.9	42.4	1.86
PC-11	50	6.2	0.3	−24.16					77.7	41.5	1.87
PC-10	70	6.4	0.39	−14.46					88.5	42.9	2.06
PC-9	90	6.6	0.31	−25.01					102	40.1	2.54
PC-8	110	6.7	0.32	−15.08					77.4	39.2	1.97
PC-7	130	7	0.37	−24.42	28.71	0.11	10025	32	76.3	40.1	1.90
PC-6	150	7.2	0.3	−24.11					78.3	37.7	2.07
PC-5	170	7.3	0.29	−24.57					76.3	35	2.18
PC-4	190	7.7	0.27	−24.51					89	34.6	2.57
PC-3	210	8	0.19	−13.6					70.5	28.2	2.50
PC-2	220	8.2	nd	nd					2.21	51.2	0.04
PC-1	nd	8.4	nd	nd					1.71	1220	0.001
XP-18	0	6.2	2.68	−10.91	104.75	0.26	Modern		nd	nd	nd
XP-17	5	6.6	2.03	−24.93					75	52.7	1.42
XP-16	10	6.6	0.72	−21.57	88.48	0.22	983	20	68.8	51.5	1.33
XP-15	20	6.5	0.66	−20.66					67.9	53.1	1.27
XP-14	30	6.4	0.41	−24.32					63.3	56.2	1.12
XP-13	50	6.4	0.4	−23.76					88.3	55	1.60
XP-12	60	6.5	0.43	−24.3					103	56.3	1.82
XP-11	70	6.7	0.38	−24.55					100	57.8	1.73
XP-10	80	6.7	0.38	−24.79	48.13	0.14	5875	24	107	58.1	1.84
XP-9	90	6.8	0.37	−24.2					103	57.8	1.78
XP-8	100	6.9	0.48	−22.5					109	60.4	1.80
XP-7	110	7.5	0.4	−24					107	59.4	1.80
XP-6	120	7.3	0.54	−24.27					110	60.2	1.82
XP-5	130	7.8	0.95	−24.59	57.33	0.18	4470	26	114	63.3	1.80
XP-4	nd	8.2	nd	nd					123	68.9	1.78
XP-3	nd	9.7	nd	nd					124	62.3	1.99
XP-2	nd	9.2	nd	nd					1.5	50.7	0.02
XP-1	nd	9.1	nd	nd					16.2	48.5	0.33
PB-20	20	5.3	1.05	−22.04	74.61	0.2	2353	21	83	54.2	1.53
PB-19	30	5.6	0.75	−19.87					82.3	54.9	1.49
PB-18	40	5.9	0.61	−20.24					80.9	54.5	1.48
PB-17	50	6.1	0.55	−22.76					84.3	55.4	1.52
PB-16	60	5.9	0.54	−22.26					80.5	52.4	1.53
PB-15	70	6	0.48	−22.33					83.8	52.9	1.58
PB-14	80	6.3	0.44	−22.44					81.8	53.3	1.53
PB-13	90	6.5	0.36	−15.2					80.8	51.5	1.56
PB-12	100	6.9	0.33	−23.25	31.94	0.13	9169	33	89.4	52.9	1.68
PB-11	110	6.9	0.41	−23.19					91.9	52.1	1.76
PB-10	120	7	0.4	−22.73					88.4	51.9	1.70
PB-9	130	7	0.46	−24.67					69.8	45.9	1.52
PB-8	140	7.1	0.45	−17.89					93.4	51.4	1.81
PB-7	150	7.1	0.45	−20.59					89	52	1.71
PB-6	160	7.1	0.39	−13.27	22.78	0.1	11885	35	88.5	52.5	1.68
PB-5	170	7.1	0.36	−22.65					105	52	2.01
PB-4	180	7.4	0.36	−16.54					108	52.3	2.06
PB-3	nd	8.8	nd	nd					3.85	74	0.05
PB-2	nd	9	nd	nd					3.43	76.7	0.04
PB-1	nd	10	nd	nd					2.2	67.9	0.03
HZB-16	0	7.6	0.78	−25.92	74.26	0.19	2390	21	98.00	46.53	2.10
HZB-15	10	6.9	3.03	−20.94					105.83	42.29	2.50
HZB-14	20	6.7	1.37	−21.68					107.86	41.52	2.59
HZB-13	30	6.7	1.05	−30.45	60.08	0.19	4093	25	104.29	41.10	2.53

Table 2. Cont.

Sample Profiles	Soil Depth (cm)	pH	TOC (%)	$\delta^{13}\text{C}$ (‰)	pMC (%)	Error (1 $\sigma$ )	$^{14}\text{C}$ Age (yrs BP)	Error (1 $\sigma$ )	Rb ( $\mu\text{g/g}$ )	Sr ( $\mu\text{g/g}$ )	Rb/Sr
HZB-12	40	6.7	0.77	−22.8					104.77	40.77	2.56
HZB-11	50	6.8	0.56	−22.8					102.17	44.04	2.32
HZB-10	60	6.9	0.39	−24.38					88.09	39.71	2.21
HZB-9	80	7	0.51	−23.37					103.58	40.59	2.55
HZB-8	100	7.2	0.52	−24.75					119.16	38.27	3.11
HZB-7	120	7.6	0.49	−24.51					123.75	36.03	3.43
HZB-6	140	7.3	0.65	−24.13	7.69	0.06	20605	63	117.52	33.30	3.52
HZB-5	160	7.1	0.55	−25.56					111.85	38.19	2.92
HZB-4	180	7.5	1.04	−22.66					134.59	37.70	3.57
HZB-3	200	7.6	0.86	−13.41					139.58	40.47	3.44
HZB-2	220	7.8	1	−25.51					120.73	40.54	2.97
HZB-1	nd	10.1	nd	nd					0.33	258.37	0.001

nd—not determined.

### 2.3. Soil Sample Preparation and Analysis

Soil samples collected were air dried at room temperature and impurities such as plant roots and other debris were removed. Soil and bedrock samples were ground with an agate mortar and ball mill and then passed through a 200-mesh (74  $\mu\text{m}$ ) sieve. Soil samples were placed in zip lock bags and test elements to include pH, total organic carbon (TOC), trace elements (Rb and Sr), carbon isotopes  $\delta^{13}\text{C}$  and  $\delta^{14}\text{C}$  were determined.

Soil pH value was determined based on soil quality issued by the International Organization for Standardization (ISO 10390:2005). Volume ratio of the treated soil and standardized water solution was 1:1. The pH value of the solution was measured by pH meter.

The content of carbon was determined quantitatively [42]. Testing was conducted at Capital Normal University's information system laboratory. Powder soil sample was pre-treated with 1 mol/L HCl, and carbonate minerals were removed [43]. Samples were later washed with deionized water until supernatant liquid pH value was neutral and then later dried at 60 °C. Approximately 100 mg of dried, sieved soil sample was used for analysis of the TOC and stable isotope contents. The TOC content was calibrated due to the loss of carbonate. The TOC content was determined by using an elemental analyzer (Elementar, Vario TOC cube, Langensfeld, Germany) with a precision of C  $\pm$  0.1% monitored with standard samples.

Trace elements parameters to include Rb and Sr were tested at the Beijing Research Institute of Uranium Geology. The trace elements contents were determined by inductively coupled plasma mass spectroscopy (HR-ICP-MS) (Element I, Finnigan MAT Company, Bremen, Germany) according to the DZ/T0223-2001 ICP-MS procedure at a temperature of 20 °C and 30% humidity [44]. The reproducibility of the trace elements measurements was tested by repetitional analyses. The analytical precision for each trace element was less than 10%.

Stable carbon isotope ratio ( $^{13}\text{C}/^{12}\text{C}$ ) was determined by using a gas isotope ratio mass spectrometer (MAT-252, Bremen, Germany). Testing was conducted by the State Key Laboratory of Environmental Geochemistry, Institute of Geochemistry. Measurements were normalized according to international standards material ( $\delta^{13}\text{C}_{\text{VPDB}}$ : 45.6‰  $\pm$  0.08‰) and expressed as delta value ( $\delta^{13}\text{C}$ ) notation (‰) relative to Vienna Pee Dee Belemnite (VPDB), whereby:  $\delta^{13}\text{C}$  (‰) =  $((^{15}\text{C}/^{12}\text{C})_{\text{sample}} - (^{13}\text{C}/^{12}\text{C})_{\text{standard}}) / (^{13}\text{C}/^{12}\text{C})_{\text{standard}} \times 1000$ ‰. Measurements of  $\delta^{13}\text{C}$  was conducted routinely with a precision of  $\pm$ 0.1‰. Samples were studied in duplicate with result differences within the range of accuracy according to the standard material measured values.

#### 2.4. The $^{14}\text{C}$ Radioisotope Determination

The accelerated mass spectrum (AMS) method was employed for  $^{14}\text{C}$  age determination. In comparison with the traditional decay counting method, the AMS method has the advantages of requiring a small sample size and offering an efficient measurement time. For this research, 3–4 samples were randomly selected from each representative profile to determine the  $^{14}\text{C}$  radioactivity ratio of the organic matter and then the apparent age calculated. The results of  $^{14}\text{C}$  dating show that the profiles maximum error of age correction was less than 63 years. The  $^{14}\text{C}$  data are reported as percent modern carbon (pMC) and as conventional  $^{14}\text{C}$  years before present (yrs. BP). The  $^{14}\text{C}$  determination test was performed and measured using the 3 MV tandem accelerator at the Xi'an AMS (XAAMS) center facility for  $^{14}\text{C}$  analysis [45]. All  $^{14}\text{C}$  data were calibrated using calibration 7.0.2 [46].

#### 2.5. Statistical Analysis

All statistical analyses were performed by Origin 8.5 (OriginLab, MA, USA). The relationships among the parameters TOC,  $\delta^{13}\text{C}$ ,  $^{14}\text{C}$  apparent age and Rb/Sr ratio with soil depth and soil pH were determined by linear regression analysis.

### 3. Results

The depth distribution of pH, total organic carbon, Rb/Sr ratios and isotopic composition ( $\delta^{13}\text{C}$ , and  $^{14}\text{C}$ ) for the studied soil profiles in the Yunnan-Guizhou plateau of southwestern China are presented in Table 2.

#### 3.1. Vertical Depth Distribution of pH, TOC, $^{14}\text{C}$ Age and Rb/Sr Ratios in Soil Profiles

As illustrated in Table 2 and Figures 4–6 the vertical distribution of pH, TOC,  $^{14}\text{C}$  age and Rb/Sr ratios vary with depth for the studied soil profiles. The pH values of the studied soil profiles ranged from 5.02 to 10.1, which are slightly acidic to slightly alkaline in nature and are typical of red limestone soil. The pH values fluctuate with increased depth for all soil profiles. Overall, after the first 20 cm topsoil layer, the pH values tend to increase with depth except for SL1 and ND profiles. The pH value reaches the maximum value at depth or in the rock layer at the rock-soil interface for most soil profiles. The SL2 soil profile recorded the lowest pH values (5.02–5.57) in comparison with the other profiles.

The TOC content for the studied soil profiles ranged from 0.149–3.03% and showed an exponential decrease with soil depth for all profiles (Table 2; Figure 4). The maximum TOC content occurred at the surface layer for all of the profiles except for the SL1 and HZB profiles. The TOC content in the subsoil layer decreased and tended to be relatively stable beyond a certain depth (50 cm). The highest TOC content was recorded in the HZB profile while the lowest content was recorded in the SL2 profile. Additionally, two profiles (XP, HZB) indicated a sample point with an abnormal increase in TOC content at depth (Figure 4).

The  $^{14}\text{C}$  apparent age for the studied soil profiles ranged from modern to 20,605 years BP, with SL1 and SL2 profiles reflecting relatively younger aged soil when compared with the other profiles. The YD and HZB profiles represent a much older soil age that extended to the late Pleistocene period. Based on the geological period the studied profiles ranged from modern through to Holocene and to late Pleistocene period (Table 2; Figures 5 and 6).

The Rb/Sr ratios indicate relatively small degrees of variation with soil depth for each of the studied soil profiles. The Rb/Sr values were  $>2$  for SL1 and SL2 profiles ranging from 3.67 to 4.05 and from 3.33 to 4.56, respectively. Conversely, the Rb/Sr values were  $<2$  for ND and YK profiles with values between 1 and 1.46 and between 0.88 and 1.07, respectively (Table 2, Figures 5 and 6). However, the Rb/Sr ratios of the other profiles—PC, XP, PB and HZB—ranged from 0.001 to 3.57.

#### 3.2. Isotopic Composition and Distribution

The  $\delta^{13}\text{C}$  isotopic composition and distribution for the studied soil profiles from the Yunnan-Guizhou plateau of southwestern China are presented in Table 2 and Figures 5



and 6. The  $\delta^{13}\text{C}$  values for the soil profiles vary in range, with some differences greater than 3‰ reflecting a change in vegetation. The  $\delta^{13}\text{C}$  values for the profiles showed vertical variations in depth distribution that ranged as follows: SL1 (−15.98 to −16.87‰), SL2 (−18.10 to −21.69‰), ND (−15.8 to −17.3‰), YK (−14.8 to −18.5‰), PC (−13.6 to −25.15‰), XP (−10.91 to −24.93‰), PB (−13.27 to −24.67‰) and HZB (−13.42 to −30.45‰) (Table 2, Figures 5 and 6). As illustrated in Figures 5 and 6, some profiles show regular depth distribution patterns of  $\delta^{13}\text{C}$  values (SL1, SL2, ND, HZB), while others indicate some abnormal outlier points (YK, PC, XP, PB). The general  $\delta^{13}\text{C}$  value trends for the soil profiles show an increase from surface to subsurface and then a decrease before it subsequently stabilizes.

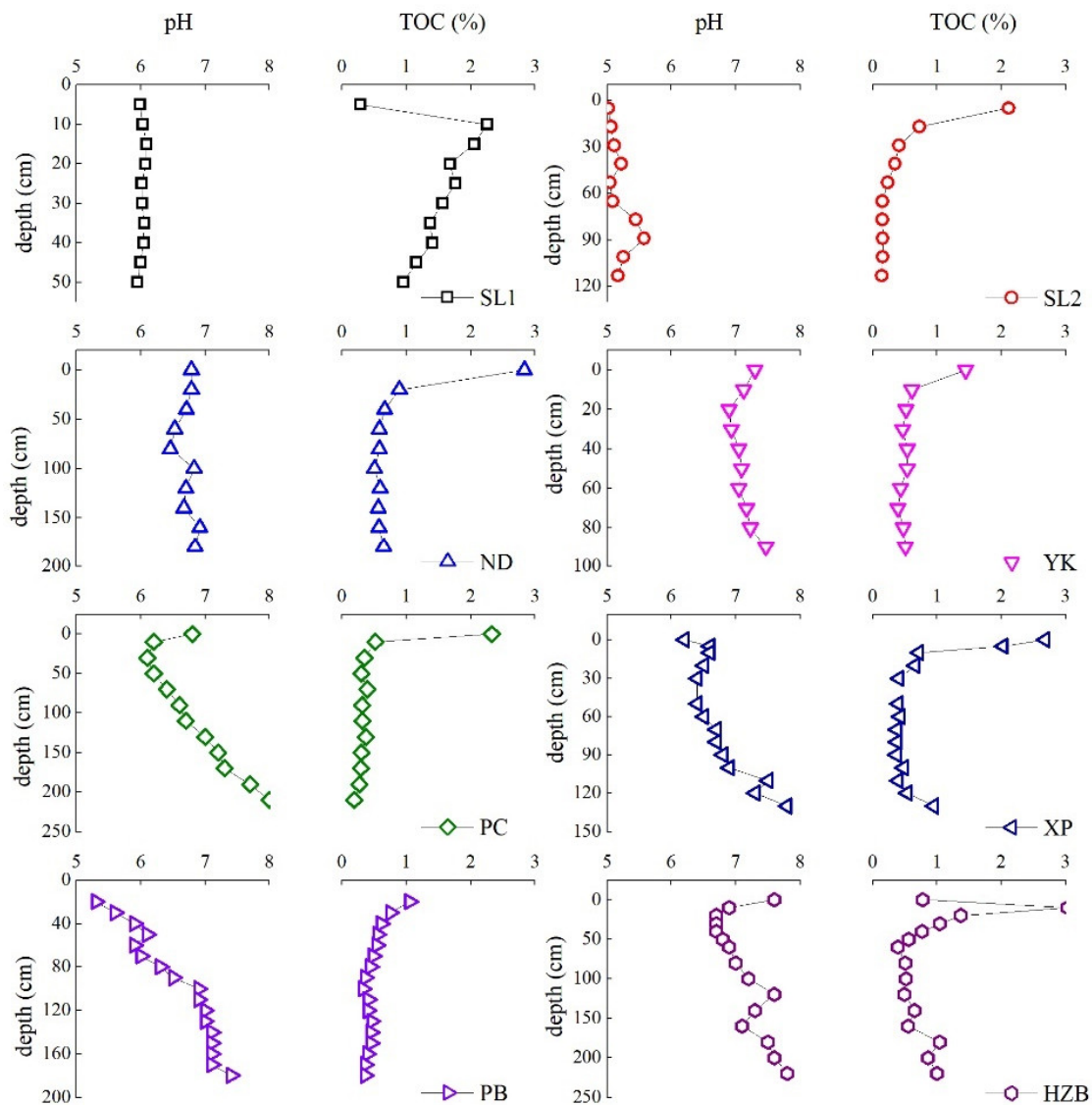


**Figure 4.** Change in pH and TOC characteristics with depth for the studied soil profiles from karst areas in the Yunnan-Guizhou plateau of southwestern China.

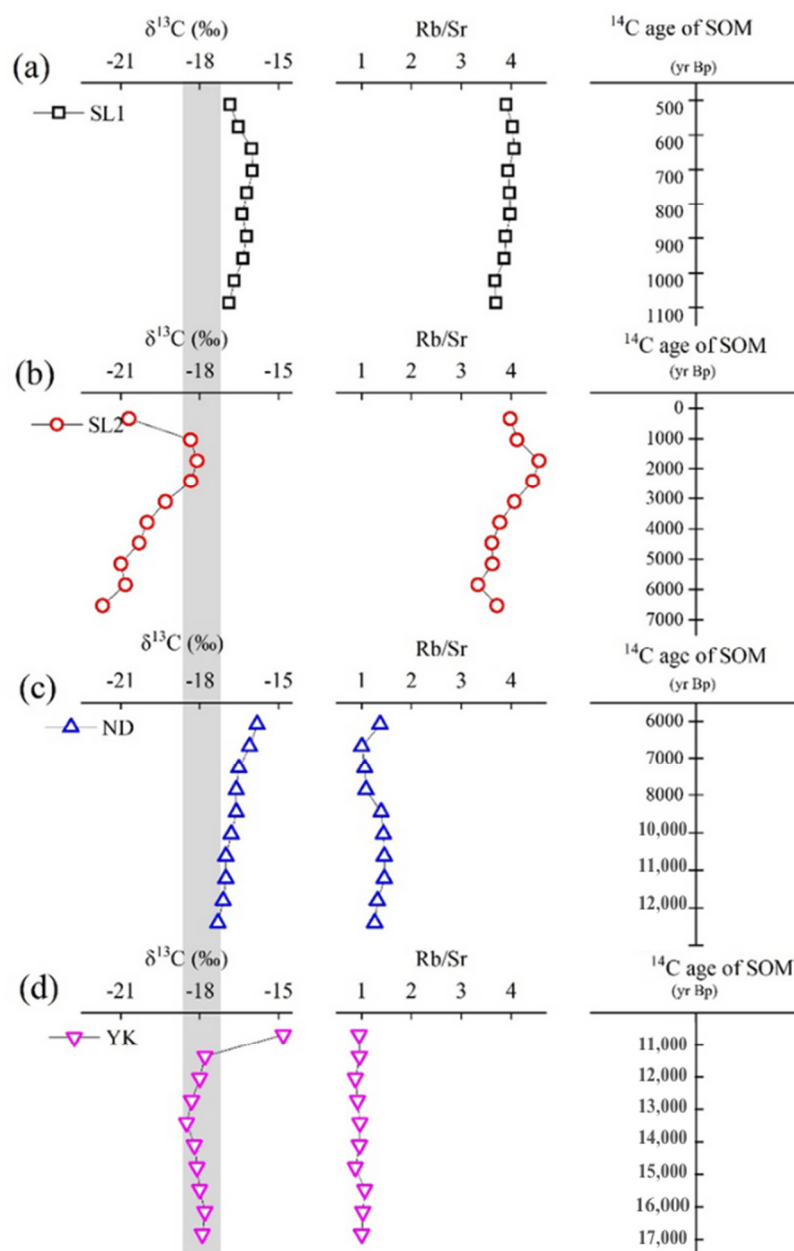


**Figure 5.** Change in  $\delta^{13}\text{C}$ ,  $^{14}\text{C}$  apparent age of soil organic matter and Rb/Sr ratios with soil depth respectively, for soil profiles (a) SL1, (b) SL2, (c) ND and (d) YK from the southwestern section of the karst areas of Yunnan-Guizhou plateau, China.

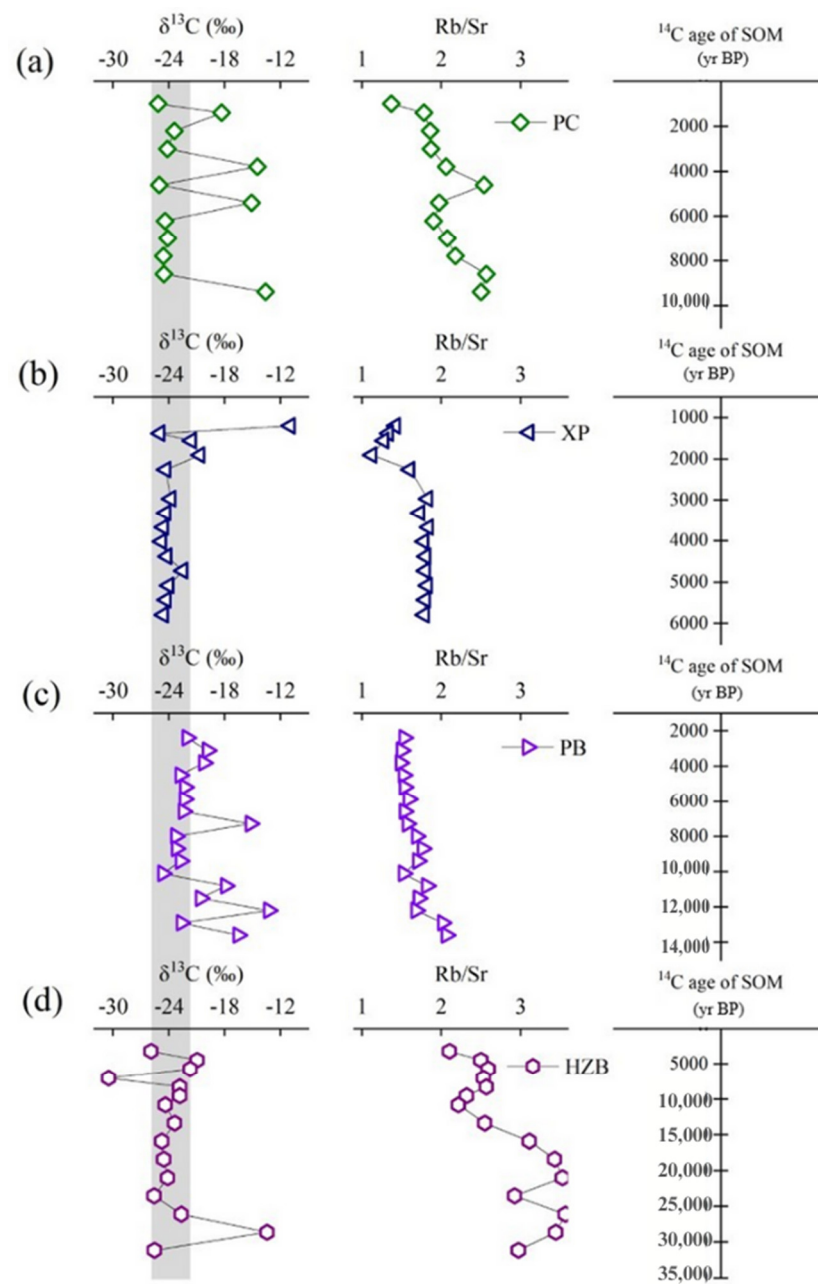


**Figure 6.** Change in  $\delta^{13}\text{C}$ ,  $^{14}\text{C}$  apparent age of soil organic matter and Rb/Sr ratios with soil depth respectively, for soil profiles (a) PC, (b) XP, (c) PB and (d) HZB from the northeastern section of the karst areas in the Yunnan-Guizhou plateau, China.

#### 4. Discussion

##### 4.1. Physiochemical Properties of Soil Profiles in Karst Environments

Hong et al., 2019 [47] have reported that soil pH is one of the major factors affecting soil nutrient availability and the elemental distribution in soil. The slightly acidic to slightly alkaline conditions reported for our soil profiles are typically characteristic of red limestone soil. Several other studies have found similar pH value ranges for southwestern China [15,48–58], primarily due to the carbonate bedrock. Our study indicates a similar distribution pattern in TOC for all of the soil profiles, with the highest TOC concentration in the surface soil layer for most profiles except for the SL1-1 profile; a rapid, exponential decrease in concentration with depth from topsoil to certain soil layers; and a relatively stable concentration after 50 cm (Figure 4). The TOC content in SL1-1 is lower than the bottom layer due to its high elevation, high rainfall and limited vegetation cover. Song

et al. 2019 [59] have reported that topographical features and vegetation cover may affect physical erosion in karst environment. The decrease in TOC with soil depth was due to the fact that there was only a small amount of residue and biomass introduced at depth and that the proportion of carbon matter in the fraction cycle decreased with depth [20,60,61]. The decrease in TOC with soil depth trend is consistent with other studies [42,62–64] and is closely related to the evolution of the soil profile [62] as well as soil microbial activities [42].

The  $^{14}\text{C}$  data for the eight studied carbonate weathering profiles are given in Table 2 and Figures 5 and 6. For all of the studied soil profiles, the topsoil had the youngest apparent age based on the  $^{14}\text{C}$  dating results, which indicates an increase with depth. Furthermore, the selected sample  $^{14}\text{C}$  age data of each profile had a strong positive linear correlation with soil depth except for the PC and XP profiles with relatively weak correlations of  $R^2 = 0.55, 0.87, 0.98, 0.97, 0.47, 0.69, 0.94,$  and  $0.97$  for SL1, SL2, ND, YK, PC, XP, PB and HZB respectively. The  $^{14}\text{C}$  data clearly recorded the effect of the translocation of shallow, more recent carbon down the soil profile, which is reflected in the soil organic matter aged increase with depth. Our results further indicate that the older soil profiles ND and YK recorded lower Rb/Sr ratios ( $<2$ ), suggesting low leaching activities, while younger SL1 and SL2 soil profiles indicate higher Rb/Sr ratios ( $>3$ ), suggesting a much high leaching and weathering degree (Figures 5 and 6). This high weathering degree was confirmed by high average chemical index of alteration (CIA) values calculated for SL1 and SL2 profiles of 95 and 96, respectively, while the other profiles average CIA values were less than 94. Variation of Rb/Sr ratio depends mainly on Sr depletion from the weathering profiles. During the weathering and leaching processes, Rb is retained in K-bearing minerals and or absorbed onto clay minerals, and is thereby reserved in weathering products, while Sr is readily released in Ca-bearing minerals and is removed by surface run-off or underground water, resulting in the observed increase in Rb/Sr ratio in the soil profiles [33]. Here, the variation in Rb/Sr ratio is due to the difference in microclimatic conditions e.g., rainfall, temperature and topography of the area. Luo [65] has reported that the regional distribution trend of annual precipitation in Guizhou province is greater in the south than in the north, and greater in the east than in the west, and that this is mainly related to topography, slope and altitude. The profiles in southern upland (SL1 and SL2) from Yunnan province has higher mean annual rainfall than the other profiles. This distribution pattern in rainfall and altitude may explain the variation in Rb/Sr ratios observed for the soil profiles within karst areas of the Yunnan–Guizhou Plateau of southwestern China (Figure 1).

#### 4.2. Stable Carbon Isotope and Vegetation History

Since most organic matter enters the soil by plant residues, the  $\delta^{13}\text{C}$  SOM value reflects stable carbon isotopic composition in plant tissues and the results of subsequent isotopic fractionation during transformation [50–53]. Soil organic matter stability depends on interactions among a wide range of biotic, abiotic and physicochemical factors controlling the rate of decomposition and stabilization [54,55]. Considerable spatial variabilities in climate and landscape, for example in altitude, can complicate this pattern [54,56]. In this study, however altitude does not seem to affect  $\delta^{13}\text{C}$  values as there was no correlation between  $\delta^{13}\text{C}$  SOM and altitude.

Stable carbon isotopes ( $\delta^{13}\text{C}$ ) of soil organic matter can be used to study vegetation changes as they reflect the contribution of C3 and C4 plants to organic matter [66]. Higher terrestrial C3 and C4 plant matter  $\delta^{13}\text{C}$  values are considered to be in the range of  $-23\text{‰}$  to  $-30\text{‰}$  or  $-21\text{‰}$  to  $-32\text{‰}$  and  $-9\text{‰}$  to  $-17\text{‰}$ , respectively [17]. Many of the studied soil profiles contain a high proportion of C3 plant material (e.g., PC, XP, PB, HZB). Only two profiles have a higher proportion of C4 plant range (e.g., SL1, ND), while the other profiles (SL2, YK)  $\delta^{13}\text{C}$  values fall in between the C3 and C4 plant range (Figure 7). The upper soil surface layer tends to reflect C3 to C4 ratios of the present vegetation [67]. It was found that C3 and C4 plants coexist in the studied profiles, which is consistent with the vegetation assessment from field investigation. Our assessment showed that the profiles vegetation

covers consist of herbs, shrub, grass, thatch, and common native species which include *Ligustrum lucidum*, *Pinus massoniana*, *Eucommia ulmoides*, *Pinus elliottii*, and *Artemisia annua*.

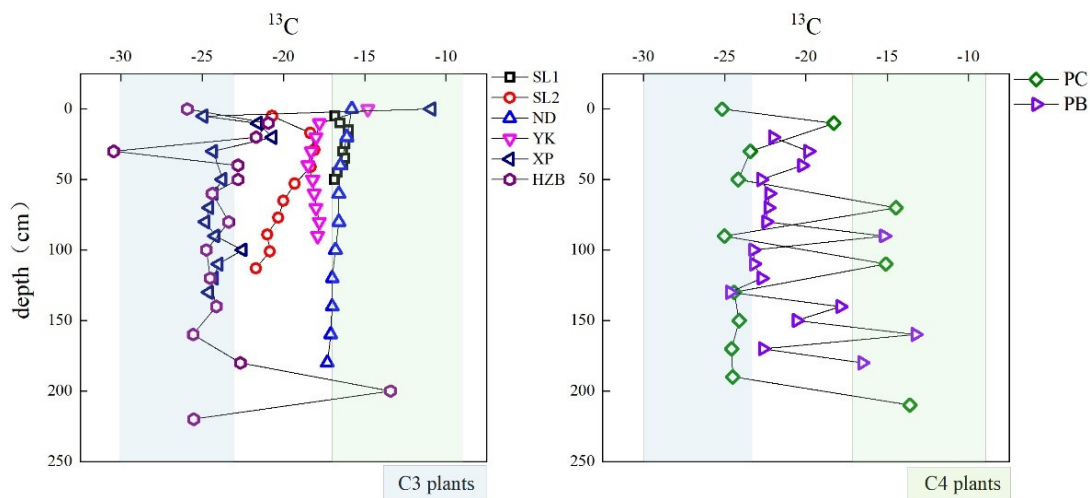


**Figure 7.** Depth distribution of  $\delta^{13}\text{C}$  showing C3 and C4 plant proportions for the sample profiles from karst areas in the Yunnan-Guizhou plateau of southwestern China.

Figure 7 shows  $\delta^{13}\text{C}$  vertical distribution for the soil profiles which indicate that the largest variation in  $\delta^{13}\text{C}$  values, i.e.,  $>3\%$ , were mainly from a small number of sample points in the C4 plant range (PC, XP, PB, HZB). According to Boutton [66], the fractionation process of carbon isotope in the soil usually causes the  $\delta^{13}\text{C}$  value to vary between 1–3‰ and any change greater than that indicates that soil organic matter contains a mixture of C3 and C4 plants. For example, the XP profile from topsoil to 5 cm, indicates that the  $\delta^{13}\text{C}$  value difference is about 14‰ (Figure 7). Based on vegetation investigation, the increase in  $\delta^{13}\text{C}$  value for the XP topsoil is due to the presence of agriculture crops (corn) in the area. The surface soil organic matter mainly comprises C4 plants, while the subsurface soil still retains the pre C3 plants that had once dominated the area. For the other abnormal points (outliers) in the profiles, e.g., PC, PB, and HZB, with a  $\delta^{13}\text{C}$  value difference greater than 3‰, it can be seen that the change may be as a result of a shift in vegetation coverage (C3 vs. C4 plants) caused by climate change and or by the influence of an external source. For the PC profile, the outlier  $\delta^{13}\text{C}$  value occurred at Stage (I), 10,500 yrs BP at points PC-3 (210 cm), PC-8 (110 cm) and PC-10 (70 cm) that are indicated in the C4 plant region (Figure 7), whereby at corresponding intervals the Rb/Sr ratios are either relatively low or there is a drastic reduction in Rb/Sr for the previous interval (Figure 6). This indicates cold and dry conditions that resulted in a shift or favorable growth of C4 plants and hence an increase in  $\delta^{13}\text{C}$  value. Similarly, for the PB profile where the outliers  $\delta^{13}\text{C}$  values occurred at sample points PB-4 (180 cm), PB-6 (160 cm) and PB-13 (90 cm) (Figure 7), the climatic conditions at that time indicate a low Rb/Sr ratio (Figure 6) with a dramatic decrease in value for the previous interval, which led to an increase in  $\delta^{13}\text{C}$  value. It is important to note however, that only one point in HZB profile i.e., HZB-3 (200 cm) had a large difference in  $\delta^{13}\text{C}$  value (Figure 6). Here the Rb/Sr ratio is relatively high and so cannot explain the increase in  $\delta^{13}\text{C}$  value that resulted in a shift towards C4 plants. Therefore, the change in vegetation at that time in history may have been caused by some other factor.

Conversely, the profiles with small  $\delta^{13}\text{C}$  value variations and with differences of 1–3‰, e.g., SL1, SL2, ND and YK (Figure 7), indicate regular patterns which are similar to other studies that have shown  $\delta^{13}\text{C}$  value increases in the upper surface and decreases in the subsurface [62,66,68,69]. This pattern is a characteristic feature of forest soils and indicates the decomposition of soil organic matter in upper soil layers by microbes [62,70]. However, the decrease in  $\delta^{13}\text{C}$  value with depth may be due to the preferential utilization of the lighter  $\delta^{13}\text{C}$  and selective preservation of plant lignin by microbes [71].

The stable carbon isotope  $\delta^{13}\text{C}$  of organic matter in the studied soil profiles revealed the coexistence of C3 and C4 plants in the soil, which is consistent with the field vegetation assessment. Large differences in  $\delta^{13}\text{C}$  value ( $>3\%$ ) were related to the cultivation of C4 crops (maize) and past climatic conditions resulted in vegetation change. Mixed vegetation that is not dominated by any one plant group (C3 and C4 plants) are quite sensitive to environmental changes and so any change in climate is reflected in  $\delta^{13}\text{C}$  value. This mixed vegetation could be used as an indicator and so future research may correlate climatic changes with vegetation changes. Stable  $\delta^{13}\text{C}$ ,  $^{14}\text{C}$  along with Rb/Sr ratio can be used to demonstrate paleoenvironmental changes in karst environments.

#### 4.3. Paleoenvironmental Interpretation from $\delta^{13}\text{C}$ , $\delta^{14}\text{C}$ and Rb/Sr Ratio

The combination of  $\delta^{13}\text{C}$ ,  $\delta^{14}\text{C}$  and Rb/Sr ratio results from eight typical red soil profiles over critical karst areas of the Yunnan–Guizhou plateau of southwestern China was analyzed and interpreted for paleoenvironmental changes (Table 2, Figures 5 and 6). Here, we used two old soil profiles (YK and ND), four intermediate profiles (XP, PC, PB, and HZB) and two young profiles (S1 and SL2) with relatively low and high variation in Rb/Sr ratio, respectively, to interpret paleoenvironmental changes. In addition, the large observed positive shift in  $\delta^{13}\text{C}$  values were considered to indicate change in C3 vs. C4 plants. This change was interpreted to be related to change in warm–wet and cold–dry climate conditions. A high  $\delta^{13}\text{C}$  value usually indicates a cold and dry climate, while low  $\delta^{13}\text{C}$  value indicates a warm and wet climate. It is well established that a cold–dry climate is more suitable for the growth of C4 plants with higher  $\delta^{13}\text{C}$  value, while a warm–wet climate is more suitable for the growth of C3 plants with lower  $\delta^{13}\text{C}$  value. The paleo soil sedimentary period of the profiles can be grouped into four to five stages starting from the bottom of the profile, i.e., stage I, through to stage V. For the ND profile the first stage, i.e., stage (I), began 11,250–8000 yrs BP (80–180 cm), which dated back to the early Holocene period. It is important to note that ND profiles comprised predominantly C4 plants with narrow ranges in  $\delta^{13}\text{C}$  value and therefore no change in vegetation (Figure 7), hence the proportional movement or direction are discussed. At stage (I) the Rb/Sr value increased and maintained relative stability at a high value later in the stage. At the same time, the  $\delta^{13}\text{C}$  value increased, the climate of the study area was mainly cold–dry, and the vegetation were mainly C4 plants. Stage (II) represents 6650–8000 yrs BP (40–80 cm). During this period the Rb/Sr ratio decreased and  $\delta^{13}\text{C}$  value increased in the middle of the Holocene era, the climate was dry and hot, and C4 plants flourished in these much-favored conditions. In stage (III), 5950–6650 yrs BP (20–40 cm), the Rb/Sr ratio decreased further and the  $\delta^{13}\text{C}$  value increased. Similar research results have been obtained from oxygen isotope records of stalagmites in Maolan, China [72], indicating dry and cold conditions. During this period the climate was mainly dry and cold reflecting more favorable conditions for C4 plants. During stage (IV), 5950 yrs BP (0–20 cm), the Rb/Sr ratio and  $\delta^{13}\text{C}$  value increased. It is inferred that the climate in the study area is mainly hot and humid, and C4 plants grow more abundantly and dominate the area. The present-day vegetation on the upper soil surface reflects C4 plants as confirmed by field investigation (Figure 7). The drastic change in Rb/Sr ratio resulted in the increase in C4 plants proportion (Figure 5).

The much older soil profile YK can be grouped into five stages. This profile comprised a mixture of both C3 and C4 plants (Figure 7) and so reflects the direction of plants proportion based on a change in environment. In the first stage of the YK profile, 15,500–17,000 yrs BP (70–90 cm), the Rb/Sr ratio increased and the  $\delta^{13}\text{C}$  value did not change significantly. It is speculated that, during this period, precipitation increased and temperature decreased, facilitating the growth of both C3 and C4 plants; however, C4 plants still dominated the vegetation. In stage (II), 14,750–15,500 yrs BP (60–70 cm), the Rb/Sr ratio decreased and the  $\delta^{13}\text{C}$  value decreased slightly. During this period the climate became dry and cold, and the proportion of C3 plants increased slightly. At stage (III), from 14,835–13,025 yrs BP (40–60 cm), the Rb/Sr ratio increased and the values of  $\delta^{13}\text{C}$  were slightly lower than the previous period (Figure 5). During this period the climate was hot and humid. Similar

results have also appeared in oxygen isotopes research, confirming that during this period the climate was hot and humid [72]. It is worth noting that, close to 14,750 yrs BP (60 cm), the Sr content and Rb/Sr ratio were higher than average. It is speculated that there may have been an extreme climatic event which caused a drastic fluctuation between 14,000–16,000 yrs BP (Figure 5). It was estimated that around 15,000 years ago, the Earth immediately started warming, this was known as a glacial termination. This resulted in the melting of the large ice sheets which covered significant parts of North America and Europe. A climatic optimum was reached shortly thereafter, around 14,700 BP, that corresponded to our present study data, and which indicated a marked drastic change in  $\delta^{13}\text{C}$  and Rb/Sr ratio in and around that time. In stage (IV), 11,845–13,025 yrs BP (20–40 cm), the Rb/Sr ratio decreased, the  $\delta^{13}\text{C}$  value slightly increased, and there was a move towards a greater proportion of C4 plants. This period was immediately after the young dryer event, was the last ice age, and was the last rapid warming in the process of the transition from the Holocene to the Pleistocene period [72,73]. During this cooling event, the largest drop in global temperature, a drop of 8 °C, occurred [73]. During this period, the reduced rainfall and the intense cooling led to the decreased proportion of C3 plants. Finally, stage (V) reflects 11,845 yrs BP (0–20 cm). In the early Holocene period, the Rb/Sr ratio first increased and then decreased and the  $\delta^{13}\text{C}$  value decreased, reflecting the growth of more dominant C4 plants. At this time the climate alternated between dry and wet, the temperature was suitable, and plants grew exuberantly. It is speculated that the climate during this period may have had alternating wet and dry conditions. The effects of the decomposition of soil organic matter by microbes on  $\delta^{13}\text{C}$  values were excluded in the interpretation.

The much younger soil profile SL1 (500–740 yrs BP), was grouped into similar intervals due to its modern age and thin soil depth. The SL1 profile was found to be predominantly composed of C4 plants, based on  $\delta^{13}\text{C}$  values (Figure 7), with little variation, indicating that there was no obvious change in vegetation history. Over the interval between 40–60 cm the Rb/Sr ratio slightly decreased, while at the same time the  $\delta^{13}\text{C}$  value increased as the C4 plants grew under the favorable conditions. At the interval 20–40 cm, the Rb/Sr ratio further increased and then slightly decreased closer to the middle section of the period. This represents a slight shift in climatic conditions with increases in rainfall and temperature followed by decreases. At the same time the  $\delta^{13}\text{C}$  value increased as C4 plants flourished then decreased, reflecting this change. At the upper 0–20 cm of the soil profile, Rb/Sr ratio decreased while the  $\delta^{13}\text{C}$  value decreased (Figures 5 and 6). This change reflects the decomposition of soil organic matter in the upper surface layer of the soil profile. Soil microorganisms preferentially utilize high nutrient and energy rich  $^{13}\text{C}$  compounds, for example polysaccharides, leaving behind substrate that are more enriched in low  $^{13}\text{C}$  and recalcitrant compounds, such as lignin [42,74].

Similarly, the SL2 soil profile (90–3040 yrs BP) is a relatively young profile which is composed of a mixture of both C3 and C4 plants with no particular group dominating (Figure 7). At the first stage of the SL2 profile (>70 cm), the Rb/Sr ratio decreased drastically then increased, suggesting initially low rainfall and dry conditions. The  $\delta^{13}\text{C}$  value increase led to a move towards the dominance of C4 plants. The second stage, 30–70 cm, indicates a continued increase in Rb/Sr ratio which was also reflected in the increase in  $\delta^{13}\text{C}$  value. The vegetation that was present at the time continue to thrive and flourished under these conditions. In the upper soil surface, 0–20 cm, the Rb/Sr ratio decreased and the  $\delta^{13}\text{C}$  value also decreased (Figures 5 and 6). It is important to note that, in the relatively young soil profile, the effects of microbes in soil decomposition affect the distribution pattern of the  $\delta^{13}\text{C}$  value.

The changes in vegetation history in relation to  $\delta^{13}\text{C}$  value, Rb/Sr ratio and age for the remaining profiles have been discussed in a previous section. The drastic change in Rb/Sr ratio corresponded to changes in the  $\delta^{13}\text{C}$  value which occurred at certain apparent age depths of the soil profiles (Figures 5 and 6). The sudden shift in C3 vs. C4 plants was linked to agricultural and external influences on the PC and HZB profiles, while changes in past climatic conditions were responsible for the recorded changes in plant group. Based

on our research, we can see that paleosols within karst environments have incorporated and stored valuable physical, biological, and chemical information about past conditions into the geological record.

#### 4.4. Effect of East Asian Summer Monsoon (EAM) and Indian Ocean Summer Monsoon (ISM) on $\delta^{13}\text{C}$ Values

The variation in  $\delta^{13}\text{C}$  values in the soil profiles along the altitudinal belt that is influenced by the East Asian summer monsoon (EAM) and the Indian Ocean summer monsoon (ISM) were examined in southwestern China (Figure 1). East Asian summer monsoons (EAM) and Indian Ocean summer monsoons (ISM) are two important monsoon systems on the Asian continent, and played an important role not only in the precipitation of the region but also for global climatic change [75]. Some areas are affected by the alternation of the two monsoons, including, according to Gao [76], southwest China. Large increases in the  $\delta^{13}\text{C}$  value range of soil organic carbon generally indicate high magnitude of  $\delta^{13}\text{C}$  fractionation and hence a higher extent of organic matter mineralization [77]. The high elevation profiles (SL1, SL2, ND, and YK) in the southwestern region indicate higher enrichment in  $\delta^{13}\text{C}$  values (average  $-18\text{‰}$ ) with a narrow isotopic range of  $3\text{--}4\text{‰}$  that are relatively constant with depth (Figure 5). On the other hand, profiles (PC, XP, PB, and HZB) from the northeastern region are heavily depleted in  $\delta^{13}\text{C}$  values (average  $-24\text{‰}$ ), with much larger isotopic ranges, and show irregular fluctuation with depth (Figure 6). The southwestern profiles are believed to be heavily influenced by Indian Ocean summer monsoons while the northeastern profiles are affected by the East Asian summer monsoon climate [78] (Figure 1). Generally, more depleted  $\delta^{13}\text{C}$  values indicate higher C3 plant composition in an ecosystem and more humid environmental conditions, while a more positive  $\delta^{13}\text{C}$  value indicates a higher proportion of C4 plants and a relatively arid environment (Figure 7).

A comparison between the  $\delta^{13}\text{C}$  value of soil organic matter in the PB and PC profiles and  $\delta^{13}\text{C}$  time series of plant organic matter in the Hani peat bog in northeastern China showed a similar tendency in the period before 5000 cal yrs BP (Figure 8). The  $\delta^{13}\text{C}$  value tends to be gradually high and then gradually low. The Hani peat bog is located in the northeastern region of the EAM domain, far away from the possible influence of ISM and mainly controlled by EAM [75]. The EAM gradually weakened before around 5000 cal yrs BP resulting in a low  $\delta^{13}\text{C}$  value. Therefore, central and northern Guizhou seems to have been mainly affected by the East Asian monsoon during the period from around 0–5000 yrs BP. At around 3400–4100 and 7500 yrs BP, the high  $\delta^{13}\text{C}$  values indicate that the climate became cold and dry in the PB and PC profiles. These two periods are consistent with the  $\delta^{18}\text{O}$  proxy records of Xiangshuiyan Cave No. 1 stalagmites in Guilin province, southern China [79]. The climate of the Guilin area is mainly affected by the EAM, therefore the decrease of PB and PC profiles precipitation in the above two periods may be related to the EAM weakening. At around 11,600 to 12,500 yrs BP, corresponding to the Younger Dryas, the  $\delta^{13}\text{C}$  values of PB soil organic matter are highest, indicating the lowest relative humidity and temperature in the center of Guizhou province. This situation can be attributed to weak summer monsoon activity, which can be considered to be widespread phenomena during the Younger Dryas, as it led to reduced precipitation and temperature or increased dry and cold climate conditions in the region [75,80,81]. The high  $\delta^{13}\text{C}$  values of the PB and PC profiles occurred at around 13,800 yrs BP, corresponding to large-scale iceberg dumping events in the north Atlantic (H1: 13,500–14,000 yrs BP) [82]. Scholars believe that, on centennial to millennial time scales, the weakening of the ISM may synchronize with abrupt ocean surface cooling in the North Atlantic [83,84]. Therefore, the high  $\delta^{13}\text{C}$  values in this period maybe affected by the change of ISM. Based on the above discussion, we speculate that the climate of central and northeastern Guizhou is mainly affected by the East Asian monsoon, but that ISM will also affect the region when the monsoon changes greatly.



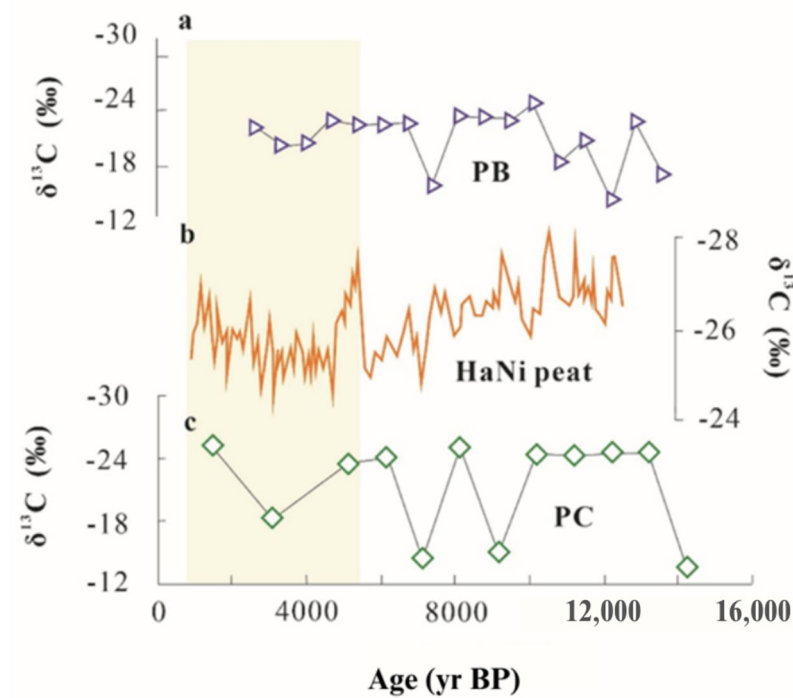


**Figure 8.** (a,c)  $\delta^{13}\text{C}$  vs.  $^{14}\text{C}$  apparent age of PB and PC soil profiles from karst areas in the Yunnan-Guizhou plateau respectively, compared with (b)  $\delta^{13}\text{C}$  time series of plant remains from the Hani peat bog in northeastern China. Data taken from Hong et al., 2005.

Hongyuan peat plant is located in the eastern region of the Tibetan plateau and its moisture content depends mainly on rainfall caused by ISM. Therefore, variation in the  $\delta^{13}\text{C}$  value of Hongyuan peat plant organic matter is closely related to changes in ISM which can be considered as a proxy indicator for the monsoon. The small  $\delta^{13}\text{C}$  value of peat plant organic matter indicates strong monsoonal activity, and vice versa [75]. The  $\delta^{13}\text{C}$  value of the HZB profile in northwestern Guizhou is compared with the  $\delta^{13}\text{C}$  of Hongyuan peat plant organic matter and the  $\delta^{18}\text{O}$  record of the Greenland Ice Sheet Project 2 (GISP2) from Greenland [85] (Figure 9). At around 28,000 yrs BP, the corresponding period of  $\delta^{18}\text{O}$  record relative increases of GISP2 and  $\delta^{13}\text{C}$  values of PB soil organic matter, indicating lower humidity and temperature. Furthermore, this also corresponds to a large-scale iceberg dumping event in the north Atlantic (H3:26,600–29,100 yrs BP) [82]. As mentioned above, the weakening of ISM may synchronize with the abrupt ocean surface cooling in the north Atlantic. Therefore, the climate became cold and dry during this period, a change which could support the notion that HZB was affected by ISM. The abnormal temperature and humidity of HZB around 1350 and 5400 yrs BP are consistent with changes of proxy recorded in Hongyuan peat. The study of carbon and oxygen isotopes in Guizhou found that the HZB area has high  $\delta^{18}\text{O}$  values. This area is considered to be strongly affected by ISM. With support from previous studies, along with our own research, it is reasonable to believe that the climate changes in western Guizhou and northern Guizhou are affected by different monsoons.

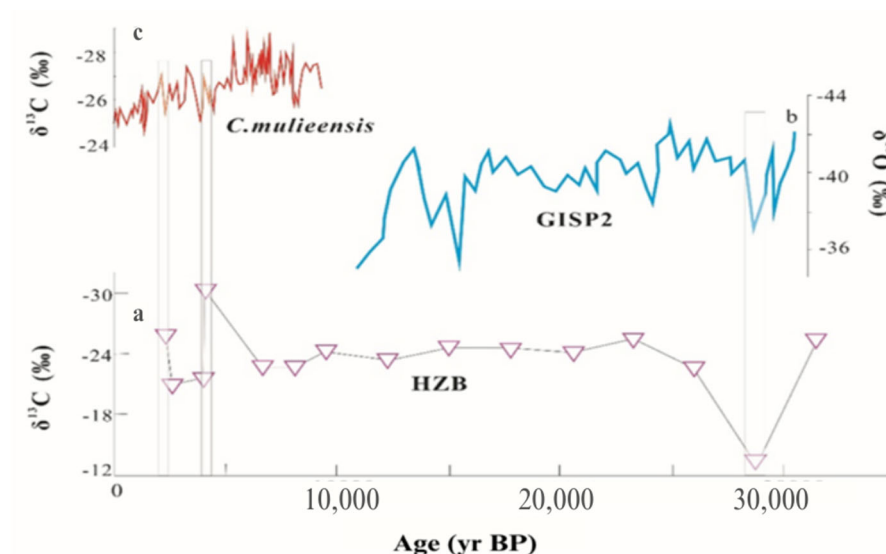


**Figure 9.** (a)  $\delta^{13}\text{C}$  vs.  $^{14}\text{C}$  apparent age of HZB soil profile from karst areas in the Yunnan-Guizhou plateau compared with (b) the  $\delta^{18}\text{O}$  record of GISP2 from Greenland and (c) the  $\delta^{13}\text{C}$  value of Hongyuan peat. Data taken from GISP2, 1997.

## 5. Conclusions

For this paper, we used  $\delta^{13}\text{C}$ ,  $^{14}\text{C}$  dating and Rb/Sr ratio to demonstrate paleoenvironmental changes in critical karst areas of the Yunnan–Guizhou plateau of southwestern China and to make the following conclusions:

The  $\delta^{13}\text{C}$  values of soil organic matter in the studied profiles revealed the coexistence of C3 and C4 plants, which is consistent with field vegetation assessment. The studied profiles found in the northeastern region had higher proportions of C3 plants (average  $-24\text{‰}$ ) and are influenced by the East Asian summer monsoon. On the other hand, soil profiles from the southwestern region had higher proportions of C4 plants (average  $-18\text{‰}$ ) that are influenced by the Indian Ocean summer monsoon climate. We found that the large differences in  $\delta^{13}\text{C}$  values were related to the cultivation of agricultural crops and changes in past climatic conditions, while the small differences were due to decomposition and translocation of SOM.

The combined results of  $\delta^{13}\text{C}$ ,  $^{14}\text{C}$  dating and Rb/Sr ratio indicate that, since the late Pleistocene, environmental conditions in the study area have changed intermittently on a millennial scale from hot–humid to cold–dry conditions. We speculate that there may have been extreme climate events in the study area during the period 14,750 yrs BP (60 cm), which was marked by drastic change in  $\delta^{13}\text{C}$  and Rb/Sr ratio. This suggests drier conditions and a move towards a higher proportion of C4 plants. Our findings show that a combination of  $\delta^{13}\text{C}$ ,  $^{14}\text{C}$  dating and Rb/Sr ratio can be used to demonstrate environmental changes in karst environment.

**Author Contributions:** Conceptualization, H.O.B.; formal analysis, H.O.B.; funding acquisition, H.J.; writing—original draft, H.O.B.; writing—review and editing, C.C., H.J. and H.O.B.; supervision, H.J. All authors have read and agreed to the published version of the manuscript.

**Funding:** This work was jointly supported by the National Natural Science Foundation of China (NSFC) grants (Nos. 41473122, 41073096), National Key Basic Research Program of China (2013CB956702) and the Hundred Talents Program of the Chinese Academy of Sciences.

**Data Availability Statement:** The data are available on request from the corresponding author.

**Acknowledgments:** The authors are indebted to Shijie Wang for suggestions and discussion about this study.

**Conflicts of Interest:** The authors have no competing interests to declare that are relevant to the content of this article.

## References

- Amundson, R.; Richter, D.D.; Humphreys, G.S.; Jobbágy, E.G.; Gaillardet, J. Coupling between Biota and Earth Materials in the Critical Zone. *Elements* **2007**, *3*, 327–332. [[CrossRef](#)]
- Leopold, M.; Völkel, J.; Dethier, D.; Huber, J.; Steffens, M. Characteristics of a paleosol and its implication for the Critical Zone development, Rocky Mountain Front Range of Colorado, USA. *Appl. Geochem.* **2011**, *26*, S72–S75. [[CrossRef](#)]
- Nordt, L.C.; Hallmark, C.T.; Driese, S.G.; Dworkin, S.I.; Atchley, S.C. Biogeochemical characterization of a lithified paleosol: Implications for the interpretation of ancient Critical Zones. *Geochim. Cosmochim. Acta* **2012**, *87*, 267–282. [[CrossRef](#)]
- Nordt, L.C.; Hallmark, C.T.; Driese, S.G.; Dworkin, S.I. Multianalytical pedosystem approach to characterizing and interpreting the fossil record of soils. In *New Frontiers in Paleopedology and Terrestrial Paleoclimatology*; Driese, S.G., Nordt, L.C., Eds.; SEPM Special Publication No. 104; SEPM: Tulsa, OK, USA, 2013; pp. 47–62. [[CrossRef](#)]
- Marin-Spiotta, E.; Chaopricha, N.T.; Plante, A.F.; Diefendorf, A.F.; Mueller, C.W.; Grandy, A.S.; Mason, J.A. Long-term stabilization of deep soil carbon by fire and burial during early Holocene climate change. *Nat. Geosci.* **2014**, *7*, 428–432. [[CrossRef](#)]
- Beverly, E.J.; Ashley, G.M.; Driese, S.G. Reconstruction of a Pleistocene paleocatena using micromorphology and geochemistry of lake margin paleo-Vertisols, Olduvai Gorge, Tanzania. *Quat. Int.* **2014**, 322–323, 78–94. [[CrossRef](#)]
- Beverly, E.J.; William EL Stinchcomb, G.E. Paleopedology as a Tool for Reconstructing Paleoenvironments and Paleoecology. In *Methods in Paleoecology*; Croft, D.A., Simpson, S.W., Su, D.F., Eds.; Reconstructing Cenozoic Terrestrial Environments and Ecological Communities, Vertebrate Paleobiology and Paleoanthropology; Springer: Berlin/Heidelberg, Germany, 2018. [[CrossRef](#)]
- Berke, M.A. Reconstructing Terrestrial Paleoenvironments Using Sedimentary Organic Biomarkers. In *Methods in Paleoecology*; Croft, D.A., Simpson, S.W., Su, D.F., Eds.; Reconstructing Cenozoic Terrestrial Environments and Ecological Communities; Springer: Cham, Switzerland, 2017; pp. 121–149.
- Cerling, T.E. Stable isotope evidence for hominin environments in Africa. In *Treatise on Geo-Chemistry*; Cerling, T.E., Ed.; Pergamon: Oxford, UK, 2014; Volume 14: Archaeology and Anthropology, pp. 157–167.
- Levin, N.E. Environment and Climate of Early Human Evolution. *Annu. Rev. Earth Planet. Sci.* **2015**, *43*, 405–429. [[CrossRef](#)]
- Nordt, L.C. Stable C and O isotopes in soils: Applications for archaeological research. In *Earth-Sciences and Archaeology*; Goldberg, P., Holliday, V., Ferring, R., Eds.; Springer: Berlin/Heidelberg, Germany, 2001; pp. 419–445.
- Sheldon, N.D.; Tabor, N.J. Quantitative paleoenvironmental and paleoclimatic reconstruction using paleosols. *Earth-Science Rev.* **2009**, *95*, 1–52. [[CrossRef](#)]
- Tabor, N.J.; Myers, T.S. Paleosols as Indicators of Paleoenvironment and Paleoclimate. *Annu. Rev. Earth Planet. Sci.* **2015**, *43*, 333–361. [[CrossRef](#)]
- Zamanian, K.; Pustovoytov, K.; Kuzyakov, Y. Pedogenic carbonates: Forms and formation processes. *Earth-Science Rev.* **2016**, *157*, 1–17. [[CrossRef](#)]
- Xi, C. On the red weathering crust of South China. *Quat. Stud.* **1991**, *11*, 103–117. [[CrossRef](#)]
- Zhu, X.M. Red residua and red soils in southern China. *Quat. Sci.* **1993**, *1*, 75–84.
- Boutton, T.W. Stable isotope ratios of natural materials: II. Atmospheric, terrestrial, marine, and freshwater environments. In *Carbon Isotope Techniques*; Coleman, D.C., Fry, B., Eds.; Academic Press: New York, NY, USA, 1991; pp. 173–185. [[CrossRef](#)]
- Trumbore, S.E. Comparison of carbon dynamics in tropical and temperate soils using radiocarbon measurements. *Glob. Biogeochem. Cycles* **1993**, *7*, 275–290. [[CrossRef](#)]
- Trumbore, S.E.; Davidson, E.; De Camargo, P.B.; Nepstad, D.C.; Martinelli, L. Belowground cycling of carbon in forests and pastures of eastern Amazonia. *Glob. Biogeochem. Cycles* **1995**, *9*, 515–528. [[CrossRef](#)]
- Trumbore, S.E. Age of soil organic matter and soil respiration: Radiocarbon constraints on belowground C dynamics. *Ecol. Appl.* **2000**, *10*, 399–411. [[CrossRef](#)]
- Pessenda, L.C.R.; Gouveia, S.E.M.; Gomes, M.B.M.; Aravena, R.; Boulet, R.; Ribeiro, A. Studies of palaeovegetation changes in the central Amazon by carbon isotopes of soil organic matter. In *Proceedings of the International Symposium on Isotope Techniques in the Study of Past and Current Environmental Changes in the Hydrosphere and Atmosphere*, Vienna, Austria, 14–18 April 1997; Murphy, P., Ed.; IAEA: Vienna, Austria, 1997.
- Pessenda, L.C.R.; Valencia, E.P.E.; Camargo, P.B.; Telles, E.C.C.; Martinelli, L.A.; Cerri, C.C.; Aravena, R.; Rozanski, K. Natural Radiocarbon Measurements in Brazilian Soils Developed on Basic Rocks. *Radiocarbon* **1996**, *38*, 203–208. [[CrossRef](#)]
- Pessenda, L.C.; Gomes, B.M.; Aravena, R.; Ribeiro, A.S.; Boulet, R.; Gouveia, S.E. The carbon isotope record in soils along a forestcarrado ecosystem transect: Implications for vegetation changes in the Rondonia state, southwestern Brazilian Amazon region. *Holocene* **1998**, *8*, 599–603. [[CrossRef](#)]
- Sanaiotti, T. The Woody Flora and Soils of Seven Brazilian Amazonian Dry Savanna Areas. Ph.D. Thesis, University of Stirling, Scotland, UK, 1996; 148p.
- Selvaraj, K.; Chen, C.T.A.; Lou, J.-Y. Holocene East Asian monsoon variability: Links to solar and tropical Pacific forcing. *Geophys. Res. Lett.* **2007**, *34*, L01703. [[CrossRef](#)]

26. Yang, T.-N.; Lee, T.-Q.; Meyers, P.A.; Song, S.-R.; Kao, S.-J.; Löwemark, L.; Chen, R.-F.; Chen, H.-F.; Wei, K.-Y.; Fan, C.-W.; et al. Variations in monsoonal rainfall over the last 21 kyr inferred from sedimentary organic matter in Tung-Yuan Pond, southern Taiwan. *Quat. Sci. Rev.* **2011**, *30*, 3413–3422. [[CrossRef](#)]
27. Chen, J.; An, Z.; Liu, L.; Ji, G.; Yang, J. The chemical composition variations of Loess Plateau dust-fall and the chemical weathering of inland Asia since 2.5 Ma. *Sci. China D* **2001**, *31*, 136–145. (In Chinese)
28. Jin, Z.; Cao, J.; Wu, J.; Wang, S. A Rb/Sr record of catchment weathering response to Holocene climate change in Inner Mongolia. *Earth Surf. Process. Landforms* **2006**, *31*, 285–291. [[CrossRef](#)]
29. Jin, Z.; Li, F.; Cao, J.; Wang, S.; Yu, J. Geochemistry of Daihai Lake sediments, Inner Mongolia, north China: Implications for provenance, sedimentary sorting, and catchment weathering. *Geomorphology* **2006**, *80*, 147–163. [[CrossRef](#)]
30. Plank, T.; Langmuir, C.H. The chemical composition of subducting sediment and its consequences for the crust and mantle. *Chem. Geol.* **1998**, *145*, 325–394. [[CrossRef](#)]
31. Bauer, A.; Velde, B.D. *Geochemistry at the Earth's Surface: Movement of Chemical Elements*; Springer: Berlin/Heidelberg, Germany; New York, NY, USA; London, UK, 2014.
32. Collins, R.N.; Kinsela, A.S. The aqueous phase speciation and chemistry of cobalt in terrestrial environments. *Chemosphere* **2010**, *79*, 763–771. [[CrossRef](#)] [[PubMed](#)]
33. Chen, J.; An, Z.; Wang, Y.; Ji, J.; Chen, Y.; Lu, H. Distribution of Rb and Sr in the Luochuan loess-paleosol sequence of China during the last 800 ka. *Sci. China Ser. D: Earth Sci.* **1999**, *42*, 225–232. [[CrossRef](#)]
34. Yuan, D.X. Karst in southwestern China and its comparison with karst in North China. *Quat. Res.* **1992**, *4*, 352–361.
35. Guizhou Provincial Geological Survey Team. *Dictionary of Stratigraphic Terms of Guizhou*; Guizhou Science and Technology Press: Guiyang, China, 1995; p. 30. [[CrossRef](#)]
36. Can, J.H.; Yuan, D.X.; Tong, L.Q. Characteristics of karst ecosystem in southwest China and comprehensive control of rocky desertification. *Grassl. Sci.* **2008**, *25*, 40–50. [[CrossRef](#)]
37. Huang, J. Yunnan Stone Forest Karst Mountain Vegetation and Soil Degradation Characteristics. Master's Thesis, Nanjing Forestry University, Nanjing, China, 2009.
38. Liu, J. Research on Karst Area Forest Vegetation Climate Characteristics. Master's Thesis, Yunnan Normal University, Kunming, China, 2015.
39. Soil Survey Staff. *Keys to Soil Taxonomy*, 12th ed.; USDA Natural Resources Conservation Service: Washington, DC, USA, 2014; pp. 161–195.
40. Ji, H.; Chang, C.; Beckford, H.O.; Song, C.; Blake, R.E. New perspectives on lateritic weathering process over karst area—Geochemistry and Si-Li isotopic evidence. *Catena* **2020**, *198*, 105022. [[CrossRef](#)]
41. Chang, C.; Beckford, H.O.; Ji, H. Indication of Sr Isotopes on Weathering Process of Carbonate Rocks in Karst Area of Southwest China. *Sustainability* **2022**, *14*, 4822. [[CrossRef](#)]
42. Zhu, S.F.; Liu, C.Q. Vertical patterns of stable carbon isotope in soils and particle-size fractions of karst areas, Southwest China. *Environ. Geol.* **2006**, *50*, 1119–1127. [[CrossRef](#)]
43. Midwood, A.J.; Boutton, T.W. Soil carbonate decomposition by acid has little effect on  $\delta^{13}\text{C}$  of organic matter. *Soil Biol. Biochem.* **1998**, *30*, 1301–1307. [[CrossRef](#)]
44. GB/T 14506.30-2010; Methods for Chemical Analysis of Silicate Rocks—Part 30: Determination of 44 Elements. National Standardization Technical Committee of Land and Resources: Beijing, China, 2011.
45. Zhou, W.; Zhao, X.; Xuefeng, L.; Lin, L.; Zhengkun, W.; Peng, C.; Wengnian, Z.; Chunhai, H. The 3MV Multi-Element AMS in Xi'an, China: Unique Features and Preliminary Tests. *Radiocarbon* **2006**, *48*, 285–293. [[CrossRef](#)]
46. Cheng, P.; Burr, G.S.; Zhou, W.; Chen, N.; Hou, Y.; Du, H.; Fu, Y.; Lu, X. The deficiency of organic matter  $^{14}\text{C}$  dating in Chinese Loess-paleosol sample. *Quat. Geochronol.* **2019**, *56*, 101051. [[CrossRef](#)]
47. Hong, S.; Gan, P.; Chen, A. Environmental controls on soil pH in planted forest and its response to nitrogen deposition. *Environ. Res.* **2019**, *172*, 159–165. [[CrossRef](#)]
48. Beckford, H.O.; Chu, H.; Song, C.; Chang, C.; Ji, H. Geochemical characteristics and behaviour of elements during weathering and pedogenesis over karst area in Yunnan-Guizhou Plateau, southwestern China. *Environ. Earth Sci.* **2021**, *80*, 61. [[CrossRef](#)]
49. Cao, X.; Wu, P.; Cao, Z. Element geochemical characteristics of a soil developed on dolomite in central Guizhou, southern China: Implications for parent materials. *Acta Geochem.* **2016**, *35*, 445–462. [[CrossRef](#)]
50. Bowling, D.R.; Pataki, D.E.; Randerson, J.T. Carbon isotopes in terrestrial ecosystem pools and  $\text{CO}_2$  fluxes. *New Phytol.* **2008**, *178*, 24–40. [[CrossRef](#)]
51. Du, B.; Liu, C.; Kang, H.; Zhu, P.; Yin, S.; Shen, G.; Hou, J.; Ilvesniemi, H. Climatic Control on Plant and Soil  $\delta^{13}\text{C}$  along an Altitudinal Transect of Lushan Mountain in Subtropical China: Characteristics and Interpretation of Soil Carbon Dynamics. *PLoS ONE* **2014**, *9*, e86440. [[CrossRef](#)]
52. Malone, E.T.; Abbott, B.W.; Klaar, M.; Kidd, C.; Sebiló, M.; Milner, A.; Pinay, G. Decline in ecosystem  $\delta^{13}\text{C}$  and mid-successional nitrogen loss in a two-century glacial chronosequence. *Ecosystems* **2018**, *21*, 1659–1675. [[CrossRef](#)]
53. Wang, C.; Wei, H.; Liu, D.; Luo, W.; Hou, J.; Cheng, W.; Han, X.; Bai, E. Depth profiles of soil carbon isotopes along a semi-arid grassland transect in northern China. *Plant Soil* **2017**, *417*, 43–52. [[CrossRef](#)]
54. Craine, J.; Fierer, N.; McLaughlan, K. Widespread coupling between the rate and temperature sensitivity of organic matter decay. *Nat. Geosci.* **2010**, *3*, 854–857. [[CrossRef](#)]

55. Zacháry, D.; Filep, T.; Jakab, G.; Molnár, M.; Kertész, T.; Király, C.; Hegyi, I.; Gáspár, L.; Szalai, Z. Carbon Isotope Measurements to Determine the Turnover of Soil Organic Matter Fractions in a Temperate Forest Soil. *Agronomy* **2020**, *10*, 1944. [\[CrossRef\]](#)
56. Zhang, D.; Hui, D.; Luo, Y.; Zhou, G. Rates of litter decomposition in terrestrial ecosystems: Global patterns and controlling factors. *J. Plant Ecol.* **2008**, *1*, 85–93. [\[CrossRef\]](#)
57. Ji, H.B.; Wang, S.J.; Ouyang, Z.Y.; Zhang, S.; Sun, C.X.; Liu, X.M.; Zhou, D.Q. Geochemistry of red residua underlying dolomites in karst terrains of Yunnan–Guizhou Plateau: I. The formation of the Pingba profile. *Chem. Geol.* **2004**, *203*, 1–27. [\[CrossRef\]](#)
58. Wei, X.; Ji, H.; Li, D.; Zhang, F.; Wang, S. Material source analysis and element geochemical research about two types of representative bauxite deposits and terra rossa in western Guangxi, southern China. *J. Geochem. Explor.* **2013**, *133*, 68–87. [\[CrossRef\]](#)
59. Song, C.; Ji, H.; Beckford, H.O.; Chang, C.; Wang, S. Assessment of chemical weathering and physical erosion along a hillslope, southwest China. *Catena* **2019**, *182*, 104133. [\[CrossRef\]](#)
60. Jobbágy, E.G.; Jackson, R.B. The vertical distribution of soil organic carbon and its relation to climate and vegetation. *Ecol. Appl.* **2000**, *10*, 423–436. [\[CrossRef\]](#)
61. Wiesmeier, M.; Spörlein, P.; Geuß, U.; Hangen, E.; Haug, S.; Reischl, A.; Schilling, B.; von Lützwow, M.; Kögel-Knabner, I. Soil organic carbon stocks in southeast Germany (Bavaria) as affected by land use, soil type and sampling depth. *Glob. Chang. Biol.* **2012**, *18*, 2233–2245. [\[CrossRef\]](#)
62. Chen, Q.Q.; Shen, C.D.; Sun, Y.M.; Peng, S.L. Mechanism of distribution of soil organic matter with depth due to evolution of soil profiles at the Dinghushan Natural Reserve. *Acta. Pedol. Sin.* **2005**, *42*, 1–8.
63. Han, G.; Li, F.; Tang, Y. Variations in soil organic carbon contents and isotopic compositions under different land uses in a typical karst area in Southwest China. *Geochem. J.* **2015**, *49*, 63–71. [\[CrossRef\]](#)
64. Liu, M.; Han, G.; Zhang, Q.; Song, Z. Variations and Indications of  $\delta^{13}\text{C}_{\text{SOC}}$  and  $\delta^{15}\text{N}_{\text{SON}}$  in Soil Profiles in Karst Critical Zone Observatory (CZO), Southwest China. *Sustainability* **2019**, *11*, 2144. [\[CrossRef\]](#)
65. Luo, W.; Wang, S.; Xie, X. A comparative study on the stable isotopes from precipitation to speleothem in four caves of Guizhou, China. *Geochemistry* **2013**, *73*, 205–215. [\[CrossRef\]](#)
66. Boutton, T.W.; Archer, S.R.; Midwood, A.J.; Zitzer, S.F.; Bol, R.  $\delta^{13}\text{C}$  values of soil organic carbon and their use in documenting vegetation change in a subtropical savanna ecosystem. *Geoderma* **1998**, *82*, 5–41. [\[CrossRef\]](#)
67. Kelly, E.F.; Amundson, R.G.; Marino, B.D.; DeNiro, M.J. Stable Carbon Isotopic Composition of Carbonate in Holocene Grassland Soils. *Soil Sci. Soc. Am. J.* **1991**, *55*, 1651–1658. [\[CrossRef\]](#)
68. Ehleringer, J.R.; Buchmann, N.; Flanagan, L.B. Carbon Isotope Ratios in Belowground Carbon Cycle Processes. *Ecol. Appl.* **2000**, *10*, 412–422. [\[CrossRef\]](#)
69. Garten, C.T.; Cooper, L.W.; Post, W.M., III; Hanson, P.J. Climate controls on forest soil C isotope ratios in the southern Appalachian Mountains. *Ecology* **2000**, *81*, 1108–1119. [\[CrossRef\]](#)
70. Powers, J.S.; Schlesinger, W.H. Geographic and vertical patterns of stable carbon isotopes in tropical rain forest soils of Costa Rica. *Geoderma* **2002**, *109*, 141–160. [\[CrossRef\]](#)
71. McCorkle, E.P.; Berhe, A.A.; Hunsaker, C.T.; Johnson, D.W.; McFarlane, K.J.; Fogel, M.L.; Hart, S.C. Tracing the source of soil organic matter eroded from temperate forest catchments using carbon and nitrogen isotopes. *Chem. Geol.* **2016**, *445*, 172–184. [\[CrossRef\]](#)
72. Qin, J.; Yuan, D.; Cheng, H.; Lin, Y.; Zhang, M.; Wang, F.; Edwards, R.L.; Wang, H.; Ran, J. Dryas and early-mid Holocene climate abrupt events: The oxygen isotope record of stalagmites in Maolan, Guizhou. *Sci. China Ser. D* **2004**, *34*, 69–74.
73. Liu, J.; Ni, Y.; Chu, G. Major climate events in the Quaternary. *Quat. Res.* **2001**, *21*, 239–248. [\[CrossRef\]](#)
74. Wynn, J.G.; Harden, J.W.; Fries, T.L. Stable carbon isotope depth profiles and soil organic carbon dynamics in the lower Mississippi Basin. *Geoderma* **2006**, *131*, 89–109. [\[CrossRef\]](#)
75. Hong, Y.; Hong, B.; Lin, Q.; Shibata, Y.; Hirota, M.; Zhu, Y.; Leng, X.; Wang, Y.; Wang, H.; Yi, L. Inverse phase oscillations between the East Asian and Indian Ocean summer monsoons during the last 12000 years and paleo-El Niño. *Earth Planet. Sci. Lett.* **2005**, *231*, 337–346. [\[CrossRef\]](#)
76. Gao, Y.X.; Xu, S.Y. *Some Problems of East Asian Monsoon*; Science Press: Beijing, China, 1962; pp. 1–49.
77. Chen, Q.Q.; Shen, C.D.; Sun, Y.M.; Peng, S.L.; Yi, W.X.; Li, Z.A.; Jiang, M.T. Spatial and temporal distribution of carbon isotopes in soil organic matter at the Dinghushan Biosphere Reserve, South China. *Plant Soil* **2005**, *273*, 115–128. [\[CrossRef\]](#)
78. Tao, F.; Hong, Y.; Jiang, H. Climatic change over the past 8000 years in Caohai District, Guizhou. *Chin. Sci. Bull.* **1997**, *42*, 409–413. [\[CrossRef\]](#)
79. Li, B.; Yuan, D.; Lin, Y.S.; Qin, Y.S.; Zhang, M.L. The Paleoclimatic Changes of Guilin Area since 40,000 a B.P. and Its Dynamical Mechanism. *Acta GeoScientia Sin.* **2000**, 21–23.
80. Gasse, F.; Arnold, M.; Fontes, J.C.; Fort, M.; Gibert, E.; Huc, A.; Li, B.; Li, Y.; Liu, Q.; Mélières, F.; et al. A 13,000-year climate record from western Tibet. *Nature* **1991**, *353*, 742–745. [\[CrossRef\]](#)
81. Lister, G.S.; Kelts, K.; Chen, K.Z.; Yu, J.Q.; Niessen, F. Lake Qinghai, China: Closed-basin like levels and the oxygen isotope record for ostracoda since the latest Pleistocene. *Palaeogeogr. Palaeoclim. Palaeoecol.* **1991**, *84*, 141–162. [\[CrossRef\]](#)
82. Bond, G.; Heinrich, H.; Broecker, W.; Labeyrie, L.; McManus, J.; Andrews, J.; Huon, S.; Jantschik, R.; Clasen, S.; Simet, C.; et al. Evidence for massive discharges of icebergs into the North Atlantic ocean during the last glacial period. *Nature* **1992**, *360*, 245–249. [\[CrossRef\]](#)

83. Gasse, F.; Van Campo, E. Abrupt post-glacial climate events in West Asia and North Africa monsoon domains. *Earth Planet. Sci. Lett.* **1994**, *126*, 435–456. [[CrossRef](#)]
84. Sirocko, F.; Garbe-Schönberg, D.; McIntyre, A.; Molfino, B. Teleconnections Between the Subtropical Monsoons and High-Latitude Climates During the Last Deglaciation. *Science* **1996**, *272*, 526–529. [[CrossRef](#)]
85. GISP2. *The Greenland Summit Ice Cores*, National Snow and Ice Data Center, [CD-ROM] ed; University of Colorado at Boulder, and the World Data Center—A for Paleoclimatology, National Geophysical Data Center: Boulder, CO, USA, 1997.

**Disclaimer/Publisher’s Note:** The statements, opinions and data contained in all publications are solely those of the individual author(s) and contributor(s) and not of MDPI and/or the editor(s). MDPI and/or the editor(s) disclaim responsibility for any injury to people or property resulting from any ideas, methods, instructions or products referred to in the content.